

# New Integrated Silicon-PDMS Process for Compliant Micro-Mechanisms

**Wisse Haouas, Redwan Dahmouche, Joël Agnus,  
Nadine Le Fort-Piat, Guillaume J. Laurent**

The authors are with FEMTO-ST Institute, AS2M department, Univ. Bourgogne Franche-Comté, UFC/CNRS/ENSMM, 24 rue Savary, 25000 Besançon, France.

## **Abstract.**

Polydimethylsiloxane (PDMS) elastomers are used for many applications, such as microfluidics and micro-engineering. This paper presents a new process of integrating soft elastomers into a silicon structure without any assembly steps. The novelty of this process is the use of only one Deep Reactive Ion Etch (DRIE) instead of two or more as developed in previous works. Thus, this fabrication process allows the use of elastomers that are usually not compatible with some fabrication processes. Compliant flexures with different interference shapes have been designed, simulated, fabricated, and characterized for generic use and notably for micro-robot joints and compliant micro-systems. The experimental results show that the  $400 \mu\text{m} \times 400 \mu\text{m}$  cross-sectional area samples can be bended more than  $60^\circ$  without delamination.

## **1. Introduction**

Micrometer-scale robotic devices with multiple degrees of freedom is a key technology in micro-manipulation and biomedical applications [1]. As the number and complexity of different mechanisms increases, microfabrication techniques have also had to evolve and be developed to support the complex requirements of these micro-devices.

Historically, Micro Electro Mechanical Systems (MEMS) were manufactured using hard materials, such as silicon, silicon dioxide, and metals [2]. Recently, there has been an increase interest into non-silicon-based MEMS, including polymers [3]. Indeed, there are a variety of microrobotic devices that require compliant elastic materials. Polyimide, parylene, and SU-8 photoresist have been used to fill the void left by traditional materials. Particularly, polydimethylsiloxane (PDMS) elastomers with their desirable properties have been widely used in the development of MEMS and microfluidic components commonly used in biomedical applications [4] [5].

Most of the fabrication processes that use PDMS either rely on soft lithography (molding) [6] [7] or patterning thin films [8]. Previous studies have been developed in literature that integrate elastomers in rigid structures, including walking [9], flying [10], and jumping robots [11] [12]. However, the development of these devices through established MEMS manufacturing approaches is hampered by the properties of traditional

silicon-based processes, such as costs and the limited set of materials, and often is limited to planar surfaces.

This paper presents a new fabrication process of hybrid microrobotic joints made of integrated silicon and PDMS. The novel fabrication process requires only one deep reactive ion etch (DRIE) although other processes need two or more DRIE steps, thus no PDMS wet etchant is required to remove the residual PDMS on the surface. This technique not only simplifies the fabrication process but also allows the use of elastomers not compatible with some fabrication processes.

The next section describes the fabrication process used to make the microrobotic joints. Section III presents some simulations for the dimensioning of the joints. Finally, the microrobotic joint characterizations and experimental results are presented in Section IV and V, respectively.

## 2. Microfabrication of Integrated Silicon/PDMS Mechanisms

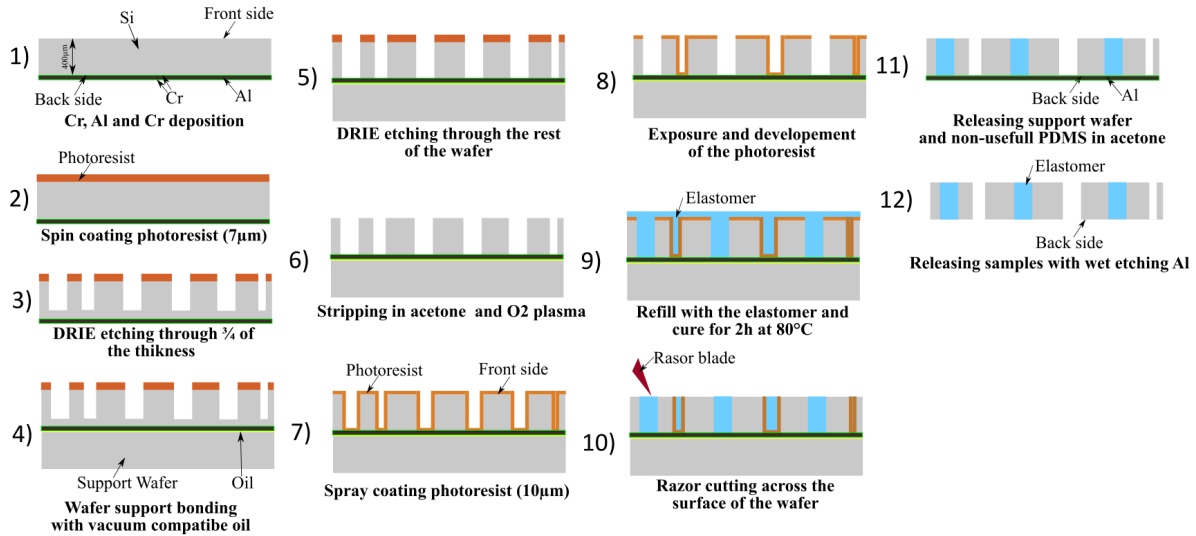


Figure 1: A schematic showing a cross section of the wafer during the microfabrication process.

Compliant mechanisms using elastic hinges generally do not suffer from friction, play, and backlash. However, the displacements are generally limited compared to the size of the mechanism [13] [14] [15]. A key challenge to overcome this issue is the addition of new materials in the currently existing micro-fabrication processes for manufacturing intricate mechanisms and substantially improving their capacities. The flexibility of some elastomers make them suitable micro-joint materials with their desirable mechanical properties (Young's modulus of approximately 2 MPa) [16].

The focus of this paper is the development of a new generic process for integrated elastomer materials into a silicon structure. The novelty came from the use of only one

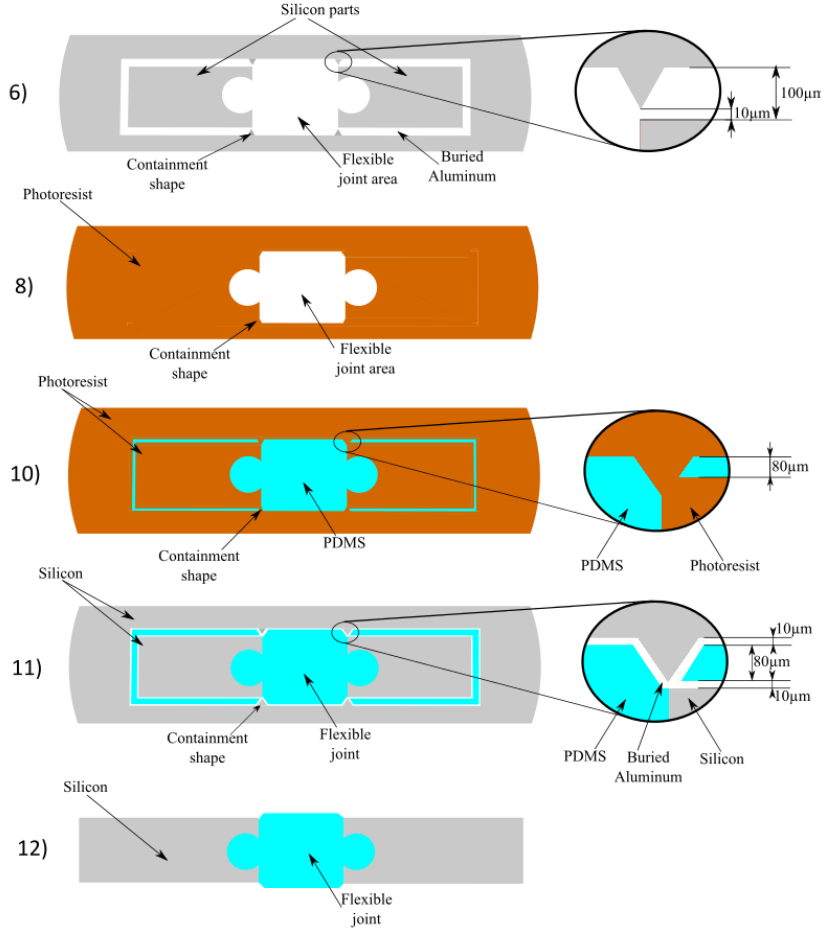


Figure 2: Top view of the wafer during some steps of the process.

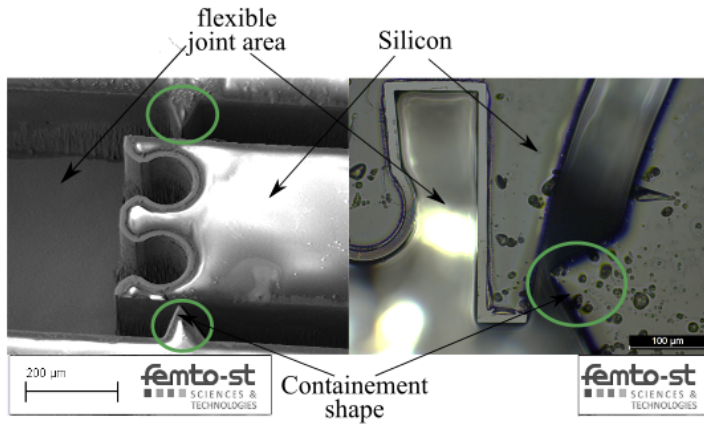


Figure 3: Scanning electron microscope (SEM) image of the etched wafer before the filling of PDMS showing the limitation shapes.

DRIE step instead of two or more as developed in [7] [17] [18].

These works typically use a mask step to define the PDMS features for the first etching. Another DRIE is performed, patterning silicon features around the elastomer

patterns. However, the small particles of elastomer left on the surface during the refilling step are removed through a rinse in n-methylpyrrolidone and tetrabutylammonium Fluoride. Following the rinse, an oxygen plasma is used to remove the residual organic materials. Finally, to release the devices, a DRIE step is performed on the backside of the wafer.

The goal of this work is to demonstrate the *in situ* micro-fabrication process that requires only one DRIE. Indeed, this technique simplifies the fabrication process and reduces the costs. To do so, the elastomer and silicon patterning features must be etched in the same step. To confine the elastomer in the flexible joint areas, a photoresist spray-coating step and a development step using an extra mask are used to define the PDMS patterns. The photoresist is used as a sacrificial layer to facilitate the removal of the unwanted pieces of elastomer. However, to avoid the releasing step using a supplementary DRIE, a fine layer of aluminum and a handling wafer are used.

This fabrication process is presented in Fig. 1 and 2. The devices are fabricated on a regular double-side polished 4" silicon wafer with a  $400 \pm 10 \mu\text{m}$  thickness. The microfabrication begins with a deposition of a thin layer of chromium (few nm), then a  $1 \mu\text{m}$  aluminum layer and finally another thin layer of chromium on the backside of a wafer (Step 1). The two layers of chromium are used to protect the aluminum layer from the developer (Steps 2 and 8). The  $1\text{-}\mu\text{m}$  layer of aluminum is adopted as a support to prevent the etched parts from moving or dropping.

In Step 2, photoresist is patterned on the front side of the device layer and the deep reactive ion etch (DRIE) step is first performed through three-quarters of the thickness of the wafer ( $300 \mu\text{m}$ ), in Step 3. The wafer is then bonded on a support wafer with vacuum compatible oil in Step 4. The DRIE step is then completed through the rest of the wafer down to the buried aluminum in Step 5. Indeed, the Steps 3 and 5 are part of the same DRIE process and could be executed in the same step by bonding the wafer support after depositing the photoresist (Step 2). Yet, the decomposition of the DRIE in two steps was made to insure better thermal conduction of the cooling system inside the vacuum chamber. The wafer is then stripped in acetone to remove the photoresist and a cleaning with an oxygen plasma is performed to remove any residual passivation layer remaining from the DRIE in Step 6.

In Step 7, a  $10\text{-}\mu\text{m}$  layer of photoresist is deposited on the front side of the wafer layer using spay coating. The photoresist is then exposed to intense UV light for the pattern and is developed to remove the exposed photoresist in the joints areas in Step 8. The wafer can then be taken out of the clean room if necessary to use elastomers that are potentially incompatible with clean room specifications. The PDMS is prohibited from some clean room facilities because of the dirtiness it can cause before polymerization.

Then, Sylgard 184 PDMS is mixed in a 10:1 ratio of the base to curing agent and degassed in a vacuum for 30 minutes. The articulation joint holes are then filled with the PDMS using a syringe. The PDMS that is filled into the wafer is then degassed to remove any air bubbles from the PDMS and to ensure that the joints that are etched in the wafer are completely refilled with PDMS. The PDMS is cured in an oven at  $90^\circ\text{C}$

for 2 hours in Step 9. The PDMS is then removed from the surface of the wafer in Step 10. This is accomplished using a razor blade as a squeegee to scrape the wafer surface. This process removes the majority of the PDMS and resist on the front surface. The remaining photoresist is used to lift off any residual PDMS.

In Step 11, a solvent is used to remove the vacuum compatible oil to separate the wafer from the handle wafer and to eliminate the photoresist and the non-useful PDMS that remains on the edge and on the surface. Finally, in Step 12, an aluminum etch is used to release the structures.

Since the elastomer and the silicon patterning features are etched in the same step, the elastomer in Step 9 will spread throughout the wafer. To confine the elastomer in the joint areas, triangular containment shapes have been designed to facilitate the removal of the unwanted pieces of PDMS as shown in Fig. 3. In Step 8, the space of  $10\text{ }\mu\text{m}$  between the triangular areas and front sidewall is filled by photoresist using spray coating as illustrated in Fig. 2. The acetone in Step 11 eliminate the photoresist; hence, the PDMS around the devices is discarded and the PDMS features are confined only in the interference shape.

The PDMS features are formed by refilling the trenches etched in Step 9 of the fabrication process. Ideally, after photoresist removal in Step 11, the elastomer should remain only in the flexible joint area, attached to the two silicon parts. However, in some cases, the PDMS around the devices remains adherent. This problem is due to the non-uniform layer of the spray coating of photoresist during Step 7 and to the dimensions of the containment shapes. The purpose of using spray coating is to get a conformal coating layer over the wafer with the etched cavities of various sizes and for the hole depth. Indeed, the result is a good uniformity layer on flat wafer. However, when spraying photoresist on the wafer with large topography, the photoresist will tend to flow, resulting in the accumulation of photoresist at the bottom and reduction at the corner of the cavities [19]. Although, the thickness and uniformity achieved are sufficient to pattern the cavities and to obtain the desired shapes of PDMS. Nevertheless, this issue can be mitigated by dimensioning the limitation shapes according to the desired elastomer features.

One of the crucial steps in the process is the stripping in acetone during Step 6. The front surface had to be cleaned perfectly for the spray coating. Thus, the vacuum compatible oil used to adhere the two wafers could be removed by solvent. Note that this manipulation step should be performed with caution. Nevertheless, the handling wafer could be bonded again in case of dropping.

### **3. Compliant Micro-joint Design**

To use this process in microrobotic mechanisms, the mechanical properties of the PDMS after the previous process must be characterized. The PDMS joints consisted of a central flexible part and two attachments, one on each end, which interface the PDMS joints

with the silicon structure. The process has the benefit of great versatility; thus, a wide variety of 2D shapes can be fabricated.

One important consideration when processing the design stage was the dimensions of the PDMS features. In this paper, the length and the cross-sectional area were chosen to realize a compliant microrobotic joint.

To validate the compliant articulation model, we performed finite element analysis (FEA) using the commercial software ANSYS (see Fig. 4). Young's modulus and Poisson's ratio of the silicon were set to 160 GPa and 0.29, respectively, and the properties of the PDMS were set to 1.4 MPa and 0.499, respectively [20] [21]. There are two boundary conditions we have considered to validate the developed model: (a) the displacement boundary condition where a given rotation input is applied at the end of the silicon linkage and (b) the fixed support, which is applied to the other end of the linkage. The expected strain from the bending angle was compared with the ultimate tensile strength of PDMS [22].

Using a rectangular PDMS articulation of 400  $\mu\text{m}$  in each side, the maximum von-Mises stress obtained with a 60° folding angle is about 1.99 MPa, which is largely below the ultimate tensile strength, shown in Fig. 4 (a).

Using the same model, a simulation of the compliant joint with 50° in torsion was applied, and the maximum obtained von-Mises stress was about 1.2 MPa. Compared to the ultimate tensile strength, no structural failure is expected at the PDMS hinge, as shown in Fig. 4 (b). Thus, the FEA simulations results show that the PDMS joints can generate large deformation in folding and torsion.

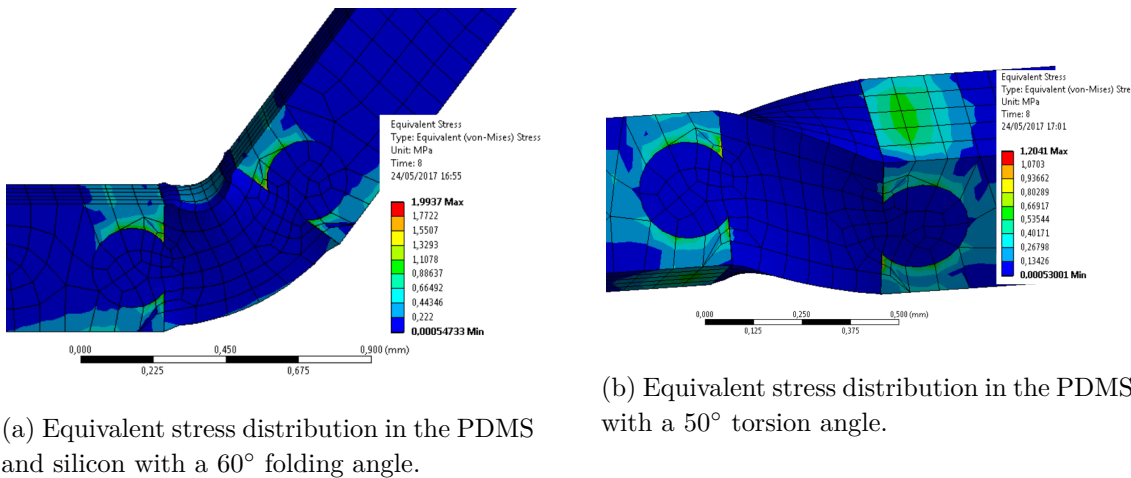


Figure 4: FEA simulation results of a three-dimensional model, which presents the robotic leg with the flexible PDMS joint. The articulation is created with a circular interference shape.

Another issue that must be addressed in this process is the robust adhesion between

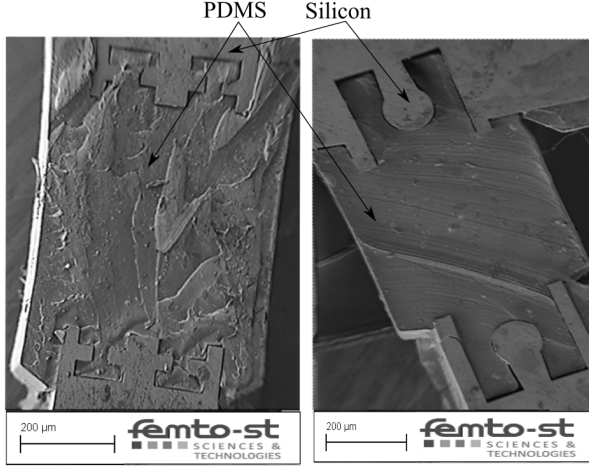


Figure 5: SEM image of a silicon and elastomer features.

the PDMS and silicon. While large deformations of the PDMS joint can be achieved, the failure of most joints comes from delamination of the PDMS from the silicon rather than the PDMS reaching its failure strain. To find the best interference shape adhesion between the PDMS and the silicon, the features in Fig. 5 were fabricated. These devices were used to determine the best silicon/PDMS adhesion feature when forces are primarily normal and perpendicular.

#### 4. Experimental Results

The compliant elastomer joints were designed to perform as a robotic articulation. Two types of tests were conducted to characterize the mechanical properties of the PDMS: tension and bending tests. This allowed a direct comparison between experimental results and simulations to determine the features that ensure the best adhesion between silicon and elastomer.

An experimental setup was used to characterize the performance of the fabricated flexible articulations in response to tension forces. For this work, we employed a high resolution camera to visualize the deformations of the PDMS in response to the forces applied using calibrated loads fixed at the end of the silicon part. The test samples are composed of 3 main parts: fixed part attached to the base, PDMS flexible joint, and hooking part where the calibrated loads are hanged (Fig. 6). The loads are industrial washers that have been weighted using a 0.01 g precision balance and hanged to generated a force directed along the F axis. The cross-sectional area of all the PDMS articulations is  $400 \mu\text{m} \times 400 \mu\text{m}$ .

The same test procedure was run on each sample, but strain achieved by the stresses varied slightly. After the tests were performed, the acquired images were processed to produce the strain-stress data (Fig. 7). The focus in this section is on the elongation phase of the tests, as shown in Fig. 8.

The results shown in Fig. 7 include four different interference PDMS/silicon features

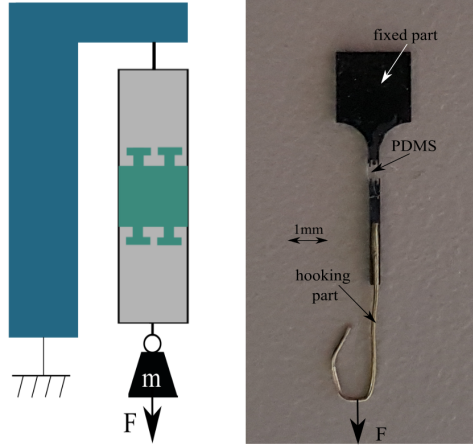


Figure 6: Image of the feature used to measure stress-strain data and the Young's modulus

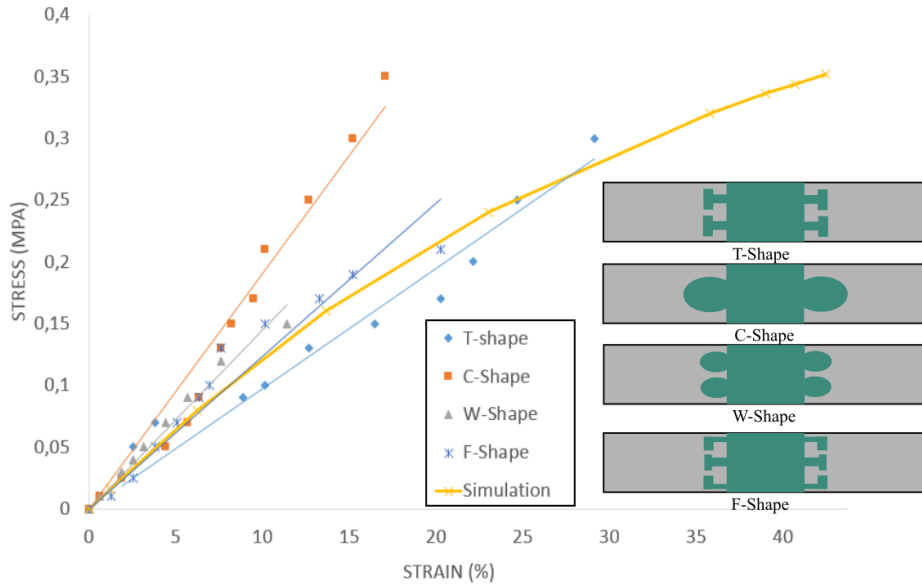


Figure 7: Stress-strain results of the PDMS samples with different interference forms compared to simulation.

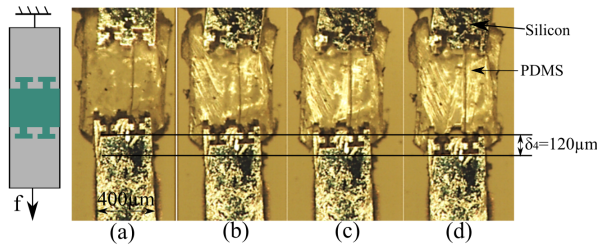


Figure 8: (a) Undefomed sample showing the attachment shapes. (b) Displacement of the PDMS feature in response to 1g, (c) 2g, and (d) 3g normal load.

for 16 samples. The multiple tested samples were from the same PDMS mixtures.

Table 1: Young's modulus for the elongation of PDMS samples compared to simulation

Shape	$E$ in MPa
T	0.97
F	1.24
W	1.45
C	1.9
Simulation	1.4

The stress-strain curves show that Young's modulus (Table. 1) varied slightly from one feature to another, although the nonlinearity of PDMS at large deformation should be considered [18].

The failure of each joint comes from delamination of the PDMS from the silicon (Fig. 9). Under normal loads, the ultimate force at which PDMS delaminated from the silicon varied from one device to another but was always above 0.15 MPa and as high as 0.35 MPa.

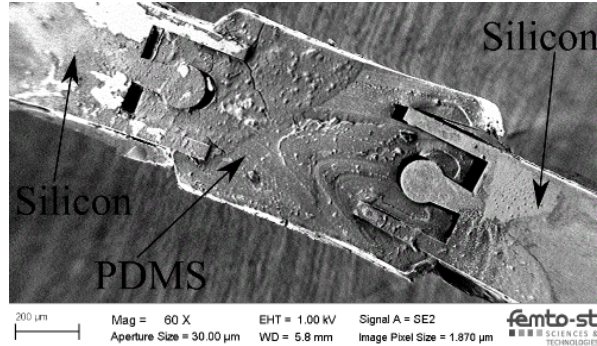


Figure 9: SEM image of a delamination of the PDMS feature from silicon.

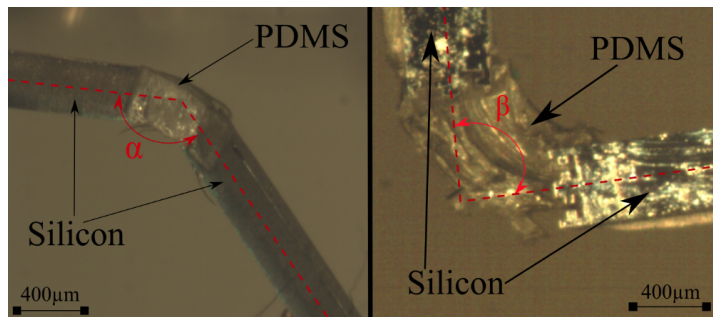


Figure 10: A PDMS joint has been folded 45° and 95° out of plane.

The compliant elastomer joints shown in Figure 10 was folded manually in order to obtain an approximate value of the maximum folding angle before delamination. For this experiment, the tested samples include a rectangular PDMS articulation of 400  $\mu$ m

in each side were folded with a probe to reach 90°. The delamination phase always occurred above 60°.

While no quantified data for the best interference features is currently available, straining of bulk PDMS in excess of 200% or 300% has been reported [9] and while a maximum strain of about 20% was reached before delamination. Increased elongation is possible if the interference features of silicon/PDMS can be improved. The fabricated devices had an average spring constant of 263 Nm<sup>-1</sup> delamination phase.

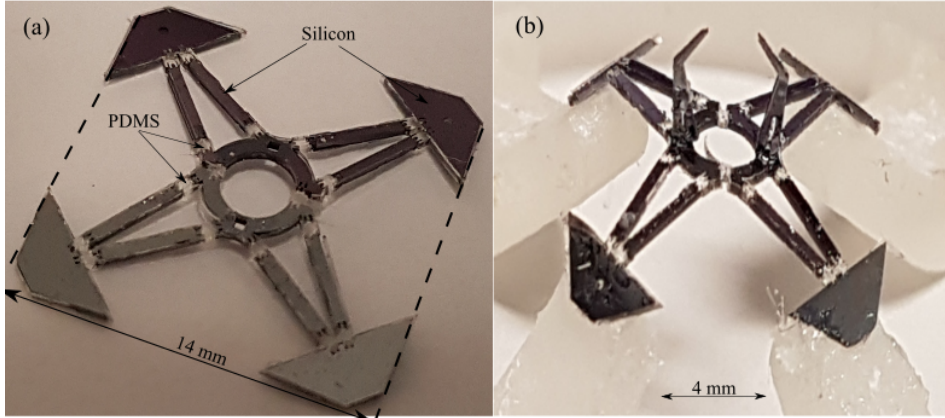


Figure 11: (a) A silicon mechanism with 18 integrated PDMS joints fabricated in plane. (b) Manipulator that is folded and fixed on four moving stages.

Using the process described above, the mechanism presented in Fig. 11 has been fabricated. The mechanism integrates 18 flexible PDMS joints and measures 14 mm on each side and 400  $\mu\text{m}$  in thickness. Every elastomer articulation is 400  $\mu\text{m}$  long, wide, and thick. The high strains and low Young's modulus of the PDMS articulations used in the mechanism compared to silicon allow for large angular deflections; hence, a large workspace could be obtained.

Overall, this process has proved to be repeatable. It could be used to fabricate shape sizes from a few micrometers to several millimeters. One issue with this fabrication process is that some of the devices were surrounded with polymer, though this excess could be easily removed at the end of the process.

## 5. Conclusion and Future Work

The compatibility with various biomedical, microfabrication, and micromachining processes, the low Young's modulus and high strains of the polydimethylsiloxane (PDMS) have made it an attractive material for use in MEMS systems. This paper presented a new process of fabrication that incorporates PDMS in a silicon wafer without the need for a post-assembly process. The novelty of this process is the use of only one DRIE instead of the two or more, usually used in such a case. Thus, the fabrication processes is simplified and allows to use elastomers not necessarily compatible with some fabrication processes or not allowed in a clean room. The process was used to fabricate

compliant hinges that could be used in microrobotic flexible joints. The experimental characterization of the fabricated PDMS articulations with several interface shapes showed that large folding angles (more than 60°) and stretching (about 20%) are reached before delamination.

One of the limitations in this proposed MEMS processing technique is that almost all devices are planar, and it is particularly difficult to assemble three dimensional structures after fabrication. Thus, the devices would be folded after releasing, to obtain an out of plane structure. Future work will focus on the exploitation of this process to fabricate actuated and controlled micro-parallel robots that will be used for micro/nano-manipulation.

## Acknowledgments

This work was supported by Région de Bourgogne Franche-Comté, Labex ACTION project (ANR-11-LABX-01-01) and Equipex ROBOTEX project (ANR-10-EQPX-44-01). The authors acknowledge the French RENATECH network and its FEMTO-ST technological facilities MIMENTO.

- [1] Kim, D.-H., Lee, M. G., Kim, B., and Sun, Y., 2005. “A superelastic alloy microgripper with embedded electromagnetic actuators and piezoelectric force sensors: a numerical and experimental study”. *Smart materials and structures*, **14**(6), p. 1265.
- [2] Petersen, K. E., 1982. “Silicon as a mechanical material”. *Proceedings of the IEEE*, **70**(5), pp. 420–457.
- [3] Liu, C., 2007. “Recent developments in polymer MEMS”. *Advanced Materials*, **19**(22), pp. 3783–3790.
- [4] Mata, A., Fleischman, A. J., and Roy, S., 2005. “Characterization of polydimethylsiloxane (PDMS) properties for biomedical micro/nanosystems”. *Biomedical microdevices*, **7**(4), pp. 281–293.
- [5] McDonald, J. C., and Whitesides, G. M., 2002. “Poly (dimethylsiloxane) as a material for fabricating microfluidic devices”. *Accounts of chemical research*, **35**(7), pp. 491–499.
- [6] Gerratt, A. P., Tellers, M., and Bergbreiter, S., 2011. “Soft polymer MEMS”. In Micro Electro Mechanical Systems (MEMS), 2011 IEEE 24th International Conference on, IEEE, pp. 332–335.
- [7] Gerratt, A. P., Penskiy, I., and Bergbreiter, S., 2010. “Integrated silicon-PDMS process for microrobot mechanisms”. In Robotics and Automation (ICRA), 2010 IEEE International Conference on, IEEE, pp. 3153–3158.
- [8] Bowden, N., Brittain, S., Evans, A. G., Hutchinson, J. W., and Whitesides, G. M., 1998. “Spontaneous formation of ordered structures in thin films of metals supported on an elastomeric polymer”. *Nature*, **393**(6681), pp. 146–149.
- [9] Bergbreiter, S., and Pister, K. S., 2006. “Elastomer-based micromechanical energy storage system”. In ASME 2006 International Mechanical Engineering Congress and Exposition, American Society of Mechanical Engineers, pp. 539–545.
- [10] Wood, R. J., 2008. “The first takeoff of a biologically inspired at-scale robotic insect”. *IEEE transactions on robotics*, **24**(2), pp. 341–347.
- [11] Churaman, W. A., Gerratt, A. P., and Bergbreiter, S., 2011. “First leaps toward jumping microrobots”. In 2011 IEEE/RSJ International Conference on Intelligent Robots and Systems, IEEE, pp. 1680–1686.
- [12] Kim, J.-S., Lee, D.-Y., Koh, J.-S., Jung, G.-P., and Cho, K.-J., 2013. “Component assembly with shape memory polymer fastener for microrobots”. *Smart Materials and Structures*, **23**(1), p. 015011.

- [13] Brouwer, D., De Jong, B., and Soemers, H., 2010. “Design and modeling of a six DOFs MEMS-based precision manipulator”. *Precision Engineering*, **34**(2), pp. 307–319.
- [14] Culpepper, M. L., and Anderson, G., 2004. “Design of a low-cost nano-manipulator which utilizes a monolithic, spatial compliant mechanism”. *Precision engineering*, **28**(4), pp. 469–482.
- [15] Shi, H., Duan, X., and Su, H.-J., 2014. “Optimization of the workspace of a MEMS hexapod nanopositioner using an adaptive genetic algorithm”. In Robotics and Automation (ICRA), 2014 IEEE International Conference on, IEEE, pp. 4043–4048.
- [16] Ebefors, T., Mattsson, J. U., Kälvesten, E., and Stemme, G., 1999. “A walking silicon micro-robot”. In Proc. Transducers’99, pp. 1202–1205.
- [17] Vogtmann, D., and Bergbreiter, S., 2014. “Magnetic actuation of ultra-compliant micro robotic mechanisms”. In 2014 IEEE/RSJ International Conference on Intelligent Robots and Systems, IEEE, pp. 809–815.
- [18] Gerratt, A. P., Penskiy, I., and Bergbreiter, S., 2013. “*In situ* characterization of PDMS in SOI-MEMS”. *Journal of Micromechanics and Microengineering*, **23**(4), p. 045003.
- [19] Pham, N. P., Scholtes, T., Klerk, R., Wieder, B., Sarro, P., and Burghartz, J., 2001. “Direct spray coating of photoresist for MEMS applications”. In Proc. SPIE, Vol. 4557, pp. 312–319.
- [20] Penskiy, I., and Bergbreiter, S., 2012. “Optimized electrostatic inchworm motors using a flexible driving arm”. *Journal of Micromechanics and Microengineering*, **23**(1), p. 015018.
- [21] Schneider, F., Fellner, T., Wilde, J., and Wallrabe, U., 2008. “Mechanical properties of silicones for MEMS”. *Journal of Micromechanics and Microengineering*, **18**(6), p. 065008.
- [22] Johnston, I., McCluskey, D., Tan, C., and Tracey, M., 2014. “Mechanical characterization of bulk Sylgard 184 for microfluidics and microengineering”. *Journal of Micromechanics and Microengineering*, **24**(3), p. 035017.